

This is the accepted manuscript made available via CHORUS. The article has been published as:

## Superfunctionalities in Nanodispersive Precipitation-Hardened Alloys

Wei-Feng Rao and Armen G. Khachaturyan

Phys. Rev. Lett. **109**, 115704 — Published 14 September 2012

DOI: [10.1103/PhysRevLett.109.115704](https://doi.org/10.1103/PhysRevLett.109.115704)

# Super Functionalities in Nano-Dispersive Precipitation Hardened Alloys

Wei-Feng Rao and Armen. G. Khachaturyan\*

Department of Materials Science and Engineering, Rutgers University, 607 Taylor Road,  
Piscataway, New Jersey, 08854, USA;

## Abstract

Although nano-dispersive precipitation hardened alloys have been intensively studied over decades as important structural materials, the possibility that these alloys may have super functional properties has been completely overlooked. As in this letter, they may have giant low-hysteretic strain responses to external stimuli if the nanosized single-domain precipitates can switch their orientation variants under applied fields. We demonstrate that the misfit-generated coherency stress can significantly reduce the variant switching barriers and may drastically decrease or even eliminate the hysteresis of the strain super responses to external stress and/or magnetic fields. These alloys can thus be functionalized as shape memory, superelastic, and/or supermagnetostrictive materials. The conditions of such functionalization are established by the interpretation-transparent analytical calculations, and confirmed by computer prototyping. In particular, the obtained results pave the way for the engineering of rare-earth free alloys with excellent magneto-mechanical and good mechanical properties.

---

\* Corresponding author. Tel.: +1 848 445 4711; fax: +1 732 445 6780.  
*E-mail address:* khach@jove.rutgers.edu (A. G. Khachaturyan).

Decades of intensive investigations of precipitation-hardened alloys have been driven by the goal of further enhancement of their mechanical properties.<sup>1,2</sup> It has been assumed as self-evident that the atomic structure of the precipitates does not change after their formation.<sup>3,4</sup> However, in the important cases wherein the low symmetry precipitate phase has multiple crystallographically equivalent orientation variants, there is no physical reason to ignore the possibility of the displacive crystal lattice rearrangement (variant switching) within nanosized single-domain precipitates under applied fields. This scenario is especially plausible when the low-symmetry phase is near the inherent lattice instabilities where the energy barriers of the variant switching are expected to be small.<sup>5-</sup>  
<sup>11</sup> Such switching should generate giant strain responses that are commensurate with the relative lattice misfits between the orientation variants. If the switching is recoverable and low-hysteretic and the applied field is stress, the result is superelasticity. It is supermagnetostriction if both precipitates and matrix are ferromagnetic and the applied field is magnetic.

The energy barriers are expected to be small when the material is soft with respect to a certain shear deformation. For example, alloys with low elastic anisotropies,  $C' = (C_{11} - C_{12}) / 2 \approx C_{44}$ , where  $C_{11}$ ,  $C_{12}$ , and  $C_{44}$  are elastic constants of the parent cubic phase, are soft with respect to any strain rotation the principal directions of the transformation strain,  $\epsilon_{ij}^o$ .<sup>12,13</sup> An example of this type material seems to be the doped TiNi-based alloys that are two-phase nanodispersions of low-symmetry clusters with superelastic behavior<sup>5-7</sup>. There are growing evidences that the recently discovered nanostructured multicomponent Ti<sub>3</sub>Nb-based alloy dubbed Gum Metal<sup>7-10</sup> also belongs to this group of materials.

In this letter, we focus on the second group of alloys with very strong elastic anisotropy ( $C' \ll C_{44}$ ) that are soft with respect to the shear strain of  $\langle 1\bar{1}0 \rangle \{110\}$ . This is a condition of the Zener instability that is, in particular, observed in the  $\beta$  phase martensitic alloys.<sup>6,11</sup> The important new result is a discovered effect of the further reduction or even vanishing of the switching energy barrier caused by the coherency stress generated by the crystal lattice misfit,  $\varepsilon_{ij}^o$ . This effect is responsible for the achievement of the recoverable low-hysteretic switching and the corresponding low-hysteretic strain response of the two-phase nanostructured alloys.

In fact, the variant switching within precipitates can be regarded as a confined martensitic transformation whose crystal lattice rearrangement is described by evolving  $\varepsilon_{ij}^o$ .<sup>12,13</sup> Generally, its theoretical characterization is a complex multi-particle problem involving elasticity of significantly non-linear (anharmonic) system of arbitrary morphology. However, as shown here, the solution of this problem has a closed analytical form for the frequently observed plate-like precipitates. The solution for the strain response is reduced to an easily interpreted algebraic equation, which is asymptotically accurate for plate-like precipitates with small thickness-to-length ratio.

For certainty, a typical particular case of precipitation of the tetragonal phase from the cubic matrix is discussed—the consideration of precipitation of other low symmetry phases can be obtained by a trivial extension. The simplest polynomial interpolation of the specific free energy is<sup>14</sup>:

$$f^{in}(\varepsilon_{ij}^o) = \frac{1}{A^2} \prod_{q=1}^3 \chi[\varepsilon_{ij}^o; \varepsilon_{ij}^{oo}(q)], \quad (1)$$

where  $\chi[\boldsymbol{\varepsilon}_{ij}^o; \boldsymbol{\varepsilon}_{ij}^{oo}(q)] = \frac{1}{2} C_{ijkl}(q) [\boldsymbol{\varepsilon}_{ij}^o - \boldsymbol{\varepsilon}_{ij}^{oo}(q)] [\boldsymbol{\varepsilon}_{kl}^o - \boldsymbol{\varepsilon}_{kl}^{oo}(q)]$ ,  $C_{ijkl}(q)$  are the elastic moduli of the  $q$ th variant of the tetragonal phase ( $q=1,2,3$ ),  $\boldsymbol{\varepsilon}_{ij}^{oo}(q)$  is the conventional eigenstrain describing the  $q$ th variant of the stress-free tetragonal phase in the cubic coordinates<sup>15</sup>, and  $A = \chi[\boldsymbol{\varepsilon}_{ij}^{oo}(1); \boldsymbol{\varepsilon}_{ij}^{oo}(2)]$  is a normalization factor. The energy (1) minimized at  $\boldsymbol{\varepsilon}_{ij}^{oo}(q)$  has the cubic symmetry with respect to  $\boldsymbol{\varepsilon}_{ij}^o$ . It reproduces the elastic moduli and approximates the intrinsic energy barriers between the orientation variants of the tetragonal phase without any arbitrary chosen fitting parameters.

The formation of coherent precipitates with a misfit strain,  $\boldsymbol{\varepsilon}_{ij}^o$ , generates coherency stress modifying the value of the energy barriers. Based on the Khachaturyan-Shatalov theory<sup>3,16</sup>, the coherency energy can be calculated by the complex analytical equation for arbitrarily-shaped elastically anharmonic inclusions. However, in the typical particular cases of plate-like precipitates, the equation for the coherency energy is reduced to:

$$f^{coh}(\mathbf{n}_0, \boldsymbol{\varepsilon}_{ij}^o) = \frac{\omega}{2} B_{ijkl}(\mathbf{n}_0) \varepsilon_{ij}^o \varepsilon_{kl}^o, \quad (2)$$

where  $\omega$  is the volume fraction of the precipitate,  $\mathbf{n}_0$  is a unit vector perpendicular to the habit plane of the plate, and  $B_{ijkl}(\mathbf{n}_0)$  is an algebraic function of  $\mathbf{n}_0$ . (See Supplementary information). Since the strain-induced interaction between plate-like precipitates is a small correction to the interfacial energy, we neglect the interaction and consider each precipitate separately, (See supplementary information). The total specific Helmholtz and Gibbs free energies of the system are thus approximated as:

$$f(\boldsymbol{\varepsilon}_{ij}^o, \mathbf{n}_0) = \omega f^{in}(\boldsymbol{\varepsilon}_{ij}^o) + 0.5\omega B_{ijkl}(\mathbf{n}_0)\varepsilon_{ij}^o\varepsilon_{kl}^o, \quad (3a)$$

$$g(\boldsymbol{\varepsilon}_{ij}^o, \mathbf{n}_0, \boldsymbol{\sigma}_{ij}^{app}) = f(\boldsymbol{\varepsilon}_{ij}^o, \mathbf{n}_0) - \omega \boldsymbol{\sigma}_{ij}^{app} \boldsymbol{\varepsilon}_{ij}^o, \quad (3b)$$

where  $\boldsymbol{\sigma}_{ij}^{app}$  is the applied stress. Both  $\boldsymbol{\varepsilon}_{ij}^o$  and  $\mathbf{n}_0$  in (3), in fact, are the long range order (lro) parameters of the system evolving during the decomposition at the elevated temperature. *Their energy-minimizing values,  $\boldsymbol{\varepsilon}_{ij}^o = \boldsymbol{\varepsilon}_{ij}^{pr}$  and  $\mathbf{n}_0 = \mathbf{n}^p$ , determine the confined atomic structures and the morphology (the orientation of the habit plane) of the coherent plate-like precipitate, respectively.* It is noted that  $\boldsymbol{\varepsilon}_{ij}^{pr}$  determining the coherency energy and the structure (and crystal lattice symmetry) of the precipitates differs from the stress-free strain,  $\boldsymbol{\varepsilon}_{ij}^{00}(q)$ .<sup>12,13</sup> In addition, the total strain of a plate-like precipitate is always an Invariant Plane Strain that usually produces monoclinic rather than tetragonal structure of the elastically constrained precipitate<sup>3</sup> (See more in supplementary information).

Figure 1 compares the energy landscapes of  $f^{in}(\boldsymbol{\varepsilon}_{ij}^o)$  and  $f(\boldsymbol{\varepsilon}_{ij}^o, \mathbf{n}^p)/\omega$ , where  $\mathbf{n}^p$  is obtained by the zero-field decomposition. It is shown that the addition of the coherency energy changes the locations of energy wells, their depths, and barriers between them. In particular, the volume change of the cubic  $\rightarrow$  tetragonal transition plays a significant role on determining the orientation of the precipitates, supplementary Fig.S1, and thus the topology of free energy landscapes, Figs. 1(b-c).

Since the precipitates are formed by the diffusion-controlled decomposition, their shapes and orientations are fixed after the diffusion is frozen at a low temperature, i.e.,  $\mathbf{n}_0 \equiv \mathbf{n}^p = const$ . Therefore, the only effect produced by the applied stress is an evolution of  $\boldsymbol{\varepsilon}_{ij}^o$  within the precipitate, which generates a macroscopic strain. The paths of evolving

$\epsilon_{ij}^o$  under uniaxial stresses applied along the  $\langle 100 \rangle$  directions are schematically shown in Figs. 1(b-c). The stress-strain responses along different evolving paths,  $\epsilon_{ij}^o = \epsilon_{ij}^o(\mathbf{n}^p, \sigma_{ij}^{app})$ , can be determined by solving the algebraic equation of  $\partial g / \partial \epsilon_{ij}^o = 0$ . The plots of the solution are shown in Figs. 2a-3a.

The coherent decomposition of an unconstrained sample,  $\sigma_{ij}^{app} = 0$ , can produce 12 types of energetically equivalent plate-like tetragonal precipitates. Their energy-minimizing transformation strains and habit-plane orientations are symmetry-related. As a result, if a uniaxial stress is applied along one of the  $\langle 100 \rangle$  directions, the strain response of a specific type of precipitates can be obtained from that of the other type by the use of symmetry relations between them. Thus the total strain of the sample is a sum of the strain of all types of precipitates multiplied by their volume fractions. Figures 2a-3a show that the stress-induced variant switching can produce giant strains comparable with  $\epsilon_{ij}^{oo}$ , and the associated hysteresis can be drastically reduced, Fig. 3a.

Usually, the early stage of precipitation of the tetragonal phase produces the so-called tweed structure consisting of plate-like nanoscale coherent inclusions within the cubic matrix.<sup>17</sup> In particular, this is the case for a precursor state of the ferromagnetic martensitic alloys<sup>18-20</sup>. The *lro* parameters for this magnetic system are the transformation strain,  $\epsilon_{ij}^o$ , and the magnetization,  $\mathbf{M}$ . Like the stress, the magnetic field,  $\mathbf{H}$ , may also provide a driving force for the switching between different orientation variants of the precipitates. Indeed, the ferromagnetic nano-precipitates and matrix are exchange coupled because the magnetic exchange correlation length is usually significantly larger than the size of nanoprecipitates. Therefore, an  $\mathbf{H}$ -field applied to the sample will

switch/rotate the magnetization of both matrix and precipitates toward  $\mathbf{H}$ . If the coupling between the magnetization direction and the direction of the orientation variant of the precipitate is sufficiently large, it consequently switches the orientation variants of nanoprecipitates and thus produces a large strain response to the  $\mathbf{H}$ -field. This extrinsic response is supermagnetostrictive because the induced strain is of the order of  $\varepsilon_{ij}^{oo}$ .

The coupling between  $\varepsilon_{ij}^o$  and  $\mathbf{M}$  is originated from the energy of magnetocrystalline anisotropy<sup>21-23</sup>:

$$f_{\varepsilon M}(\mathbf{m}, \varepsilon_{ij}^o) \approx -\lambda m_i m_j \varepsilon_{ij}^o, \quad (4)$$

where  $\lambda = K / \varepsilon_c$ ,  $K$  is the magnetocrystalline anisotropy constant<sup>21-23</sup>, and  $\mathbf{m} = \mathbf{M} / M$  is a unit vector along  $\mathbf{M}$ . It is noted that the energy (4) has the same form of the conventional magnetoelastic coupling energy,<sup>[24]</sup> and it can be derived from the conventional form of the magnetocrystalline anisotropy,  $f_{\varepsilon M} = K[1 - (\mathbf{m} \cdot \mathbf{e})^2]$ ,<sup>[21]</sup> by a shifting of the reference state, where  $\mathbf{e}$  is a unit vector along the tetragonality axis.

If we interpret  $\sigma_{ij}^{mag} = \lambda m_i m_j$  as a “magnetic stress”, the energy (4) plays the same role as the stress energy term in (3b),  $-\sigma_{ij}^{app} \varepsilon_{ij}^o$ . Therefore, both the stress-induced and  $\mathbf{H}$ -induced strain responses of plate-like precipitates are described by the same equation (3b). However, unlike the mechanical stress that can easily reach the switching threshold, the magnetic stress,  $\sigma_{ij}^{mag} = \lambda m_i m_j$  can reach it only if  $K$  is sufficiently large. Another difference is that  $\sigma_{ij}^{mag}$  in (4) cannot change sign: it is always either negative (compressive) or positive (tensile). The calculated “magnetic stress”-strain curves suggest that such ferromagnetic nanodispersions can really have the giant magnetostriction and



small hysteresis (Figs. 2b and 3b). It is noted that the values of  $K$  used in the calculation is of the same order of the experimentally observed ones.<sup>22,23</sup>

It turns out that the analytical results obtained for the plate-like precipitates are quite general: we essentially obtained the same H-induced strain responses of ferromagnetic nanodispersions in the 3D computer modeling (Fig.4) where no *a priori* constraints on the shape and arrangement of the precipitates were imposed, and all relevant physically relevant energies were taken into account<sup>25</sup>. Fig. 4 shows that the variant switching generating large strains can take place in nanodispersions at a much smaller **H**-field (comparing to that required for the single-phase tetragonal crystals).

In this letter, the theory of coherent inclusions has been advanced by taking into consideration the principally anharmonic character inherent to multi-variant precipitates in the frequent cases of alloys with a large misfit between the phases (1~10%). We demonstrated that the two-phase nanostructured alloys can have giant low-hysteretic strain responses generated by a variant switching within single-domain coherent nanoprecipitates (Figs. 2-4). Depending on the system, this results in the shape memory effects, superelasticity and/or supermagnetostriction. All of them are new effects for otherwise well studied precipitation hardened alloys. In principle, such super functionalities could be obtained in any nanodispersion of a low-symmetry phase if the system is sufficiently hardened to prevent the competing processes such as the dislocation plasticity and fracture ( $K$  should also be sufficiently large in ferromagnetic alloys, see supplementary Figs. S3-S4).

The topology of the free energy surfaces exemplified in Fig. 1 is a key factor determining the characteristics of the strain responses. The global and local minima of the energy surfaces describe the stable and metastable orientations variants of precipitates.

The switching between them generating a large strain is generally hysteretic because it requires surmounting of the energy barriers (the saddle points separating the energy wells corresponding to different variants). To reduce or even eliminate the hysteresis, the switching barriers should be minimized. We have demonstrated that the coherency stress qualitatively changes the configurational energetics of the nanodispersions in materials with relatively low intrinsic barriers, reducing or even eliminating the switching barriers and thus the hysteresis (Figs. 2-3). For example, it could be the case for a precursor state of some decomposing  $\beta$  phase martensitic alloys ( $C' \ll C_{44}$ ) approaching the Zener instability<sup>11,26,27</sup> at temperatures above but close to the martensitic temperature,  $M_s$ . In this case, the formed tweed-like microstructure<sup>17-20</sup> is produced by the pseudospinodal mechanism<sup>28,29</sup> and consists of single-domain plate-like nanoprecipitates. It follows from the obtained results that the hysteresis can be further reduced if the formation of optimized nanostructures is promoted by proper thermo-mechanical and/or thermo-magnetic treatments.

The supermagnetostrictive state of ferromagnetic alloys can be similarly obtained by pseudo-spinodal decomposition producing tweed-like nanostructures. Promising systems to observe this effect is Fe-30at.%Pd alloys that have about 7-fold elastic softening of  $C'$  and precursor tweed-like structure consisting of single-domain precipitates of the tetragonal phase<sup>18,20</sup>. In fact, the giant magnetostriction can be anticipated in a wider class of the martensitic ferromagnetic shape memory alloys<sup>19,22,23,30,31</sup> in a frequently observed precursor two-phase nanostructured state: (i) these alloys can also have the nano-scale tweed-like nanostructure above  $M_s$ ,<sup>18-20</sup> (ii) their ferromagnetic nano-particles and matrix are exchanged coupled, (iii) they are

elastically highly anisotropic with  $C' \ll C_{44}$ , and (iv) the underlying single-domain ordered tetragonal phase usually has large value of  $K$ .<sup>22,23</sup> As suggested by Fig. 4, these materials can have giant low-hysteretic strain responses to relatively small  $\mathbf{H}$ -fields.

The authors gratefully acknowledge the support from DOE under grant DE-FG02-06ER46290 and from NSF under grant [DMR-0704045](#). The parallel computer simulations were performed on LoneStar at Texas Advanced Computing Center.

## References

1. A.J. Ardell, *Metall. Trans.* **16A**, 2131 (1985).
2. Z. Horita, K. Ohashi, T. Fujita, K. Kaneko and T.G. Langdon, *Adv. Mater.* **17**, 1599 (2005).
3. A.G. Khachaturyan, *Theory of structural transformations in solids*. (Wiley & Sons, New York, 1983).
4. J.D. Eshelby, *Solid State Phys.* **3**, 79 (1956).
5. S Sarkar, X. Ren and K. Otsuka, *Phys. Rev. Lett.* **95**, 205702 (2005).
6. K. Otsuka and X Ren, *Prog. Mater. Sci.* **50**, 511 (2005).
7. W.F. Rao and A.G. Khachaturyan, *Acta Mater.* **60**, 443 (2012).
8. T. Saito *et al.* *Science*, **300**, 464 (2003).
9. J.W. Morris *et al.* *Acta Mater.* **58**, 3271 (2010).
10. T. Yano, Y. Murakami, D. Shindo, Y. Hayasaka and S. Kuramoto, *Scripta Mater.* **63**, 536 (2010).
11. C. Zener, *Phys. Rev.*, **71**, 846 (1947).
12. W.F. Rao, M. Wuttig and A.G. Khachaturyan, *Phys. Rev. Lett.* **106**, 105703 (2011).
13. W.F. Rao and A.G. Khachaturyan, *Acta Mater.* **59**, 4494 (2011).
14. E.K.H. Salje, *Phase transformations in ferroelastic and co-elastic crystals*. (Cambridge University Press, Cambridge, 1993).
15.  $\varepsilon_{ij}^{oo}(q)$  is a diagonal tensor with one principal value along the c-axis,  $\varepsilon_c = (c_t - a_c)/a_c$ , and two equal principal values,  $\varepsilon_a = (a_t - a_c)/a_c$ , along the a-axes, where  $c_t$ ,  $a_t$  and  $a_c$  are the crystal lattice parameters of the tetragonal and cubic phases, respectively.
16. A.G. Khachaturyan and G.A Shatalov, *Sov. Phys. JETP*, **29**, 557 (1969).
17. L.E. Tanner, *Philos. Mag.* **14**, 111 (1966).
18. H.D. Chopra and M. Wuttig, *J. Phys. IV, Colloque C8*, **C8/157** (1995).
19. B. Bartova, N. Wiese, D. Schryvers, N. J. Chapman, and S. Ignacova, *Acta Mater.* **56**, 4470 (2008).
20. E.D. Cantando, G.M. Ludtka, G. Machiewicz-Ludtka and W.A. Soffa, *Solid State Phenom.* **172-174**, 356 (2011).
21. Y.M. Jin *et al.*, *J. Appl. Phys.* **92**, 6172 (2002).
22. R. Tickel and R.D. James, *J. Magn. Magn. Mater.* **195**, 627 (1999).
23. H. Morito *et al.*, *Appl. Phys. Lett.* **81**, 1657 (2002).

24. G. Engdahl, *Handbook of Giant Magnetostrictive Materials*. (Academic Press, San Diego, 2000).
25. Including the chemical bulk free energy, interfacial energy, magneto-elastic and magneto-mechanical coupling energies, coherency energy, magnetostatic energy, exchange energy, and Zeeman energy. See supplementary information for details.
26. S. Muto, R. Oshima and F.E. Fujita, *Acta Metall. Mater.* **38**, 685 (1990).
27. V.A. Chernenko, *Scripta Mater.* **40**, 523 (1999).
28. Y. Ni and A.G. Khachaturyan, *Nature Mater.* **8**, 410 (2009).
29. Y. Ni, W.F. Rao and A.G. Khachaturyan, *Nano Lett.* **9**, 3275 (2009).
30. R.D. James, and M. Wuttig, *Philos. Mag. A* **77**, 1273 (1998).
31. K. Ullakko, J.K. Huang, C. Kantner, R.C. O'Handley and V.V. Kokorin, *Appl. Phys. Lett.* **69**, 1966 (1996).

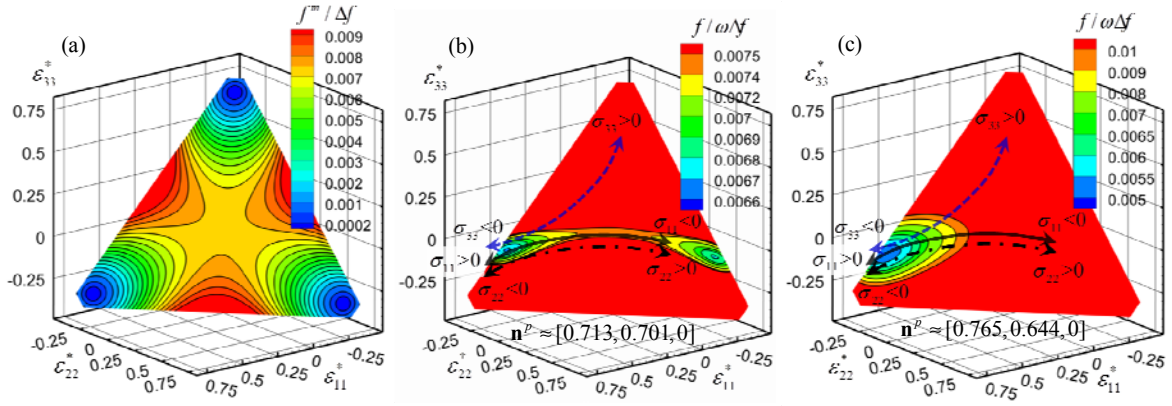


**Figure 1.** Intrinsic and the Helmholtz free energies in the planes of  $\varepsilon_{ii}^* = 0$  (a-b), and  $\varepsilon_{ii}^* = 1/7$  (c), where a large elastic anisotropy is used ( $C' = 0.1C_{44}$ ), and the strain and the energy are reduced by  $(\varepsilon_c - \varepsilon_a)$  and  $\Delta f = C_{44}(\varepsilon_c - \varepsilon_a)^2$ , respectively. The energy states significantly away from the visualized planes are much higher, and the intrinsic free energy of the case of  $\varepsilon_{ii}^* = 1/7$  is similar to (a) (See supplementary Fig. S2). In (b-c), three variant switching paths of the calculated precipitate under a uniaxial stress applied along the  $\langle 100 \rangle$  directions are demonstrated. Comparing to (a), the energy barriers along the possible switching paths in (b-c) are dramatically reduced or even diminished (single-well configuration along the paths).

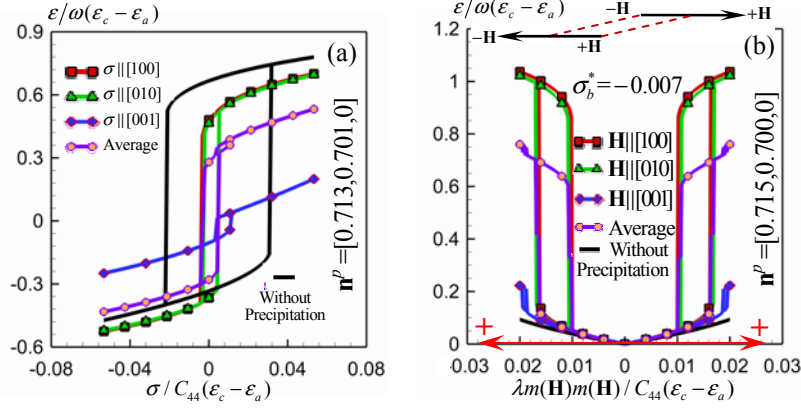


**Figure 2.** Calculated longitudinal strain responses of a cubic→tetragonal phase precipitation without volumetric effect ( $\varepsilon_{ii}^* = 0$ ) to differently oriented uniaxial stresses (a), and magnetic fields (b). The “Average” curves are the averages of the responses to fields applied along three  $\langle 100 \rangle$  directions. In (b), the positive (tensile) magnetic stress,  $\lambda^* = \lambda / C_{44}(\varepsilon_c - \varepsilon_a) = 0.02$ , is assumed of the same order of the experimentally observed  $K^{23,24}$ , ( $\sim 10^5 \text{ J/m}^3$ ), and a constant bias compression,  $\sigma_b^* = \sigma / C_{44}(\varepsilon_c - \varepsilon_a)$ , is applied along the same direction of the  $\mathbf{H}$ -field. The horizontal axis in (b) is the magnetic stress. The change of  $\mathbf{H}$ -field during the cycling is schematically shown on the top of (b). The stress-strain hysteresis of nondispersions in (a) is significantly reduced when comparing to that of the homogeneous tetragonal phase (without precipitation).

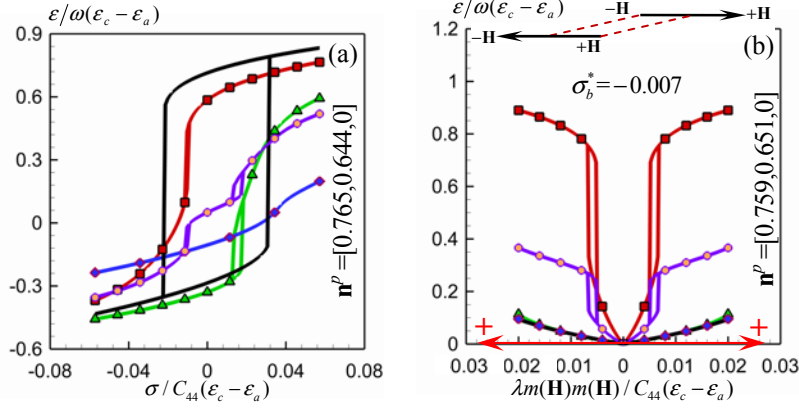


**Figure 3.** Calculated longitudinal strain responses of a cubic  $\rightarrow$  tetragonal phase precipitation with a volumetric effect ( $\varepsilon_{ii}^* = 1/7$ ) to differently oriented uniaxial stresses (a), and magnetic fields (b). Except for the volumetric effects, all other parameters used here are the same as in Fig. 2, (see Fig. 2 for the legends). It is noted that the switching induced strain response of the considered type of precipitates to a stress along the [100] direction is giant and nonhysteretic, (a), and the  $\mathbf{H}$ -induced switching produces large strain response with small hysteresis, (b).



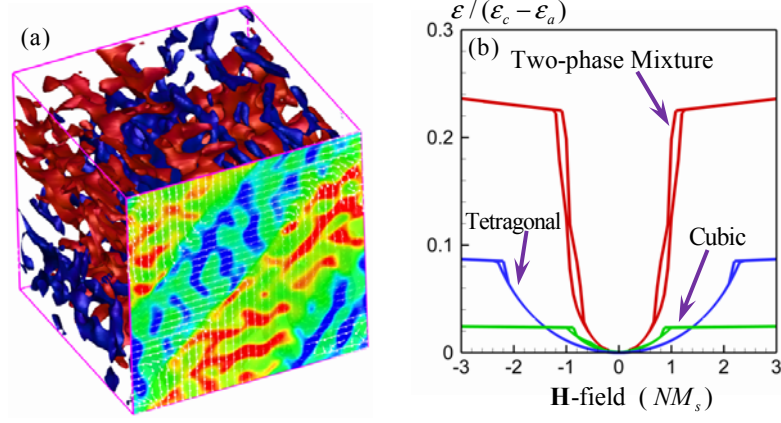


**Figure 4.** Simulated 3D microstructure of a ferromagnetic alloy and its longitudinal strain response to a magnetic field under a biased compression. The computer prototyping was performed with the same material constants and loading procedures as in Fig. 3b. (See supplementary information) In (a), the sizes of the precipitates are on the order of  $\sim 10$  nm, and the shapes of nanoprecipitates deviate from the ideal platelets because all physically relevant energies have been taken into account.<sup>25</sup> In (b),  $M_s$  and  $N$  are the saturation magnetization and the demagnetization factor determined by the shape of the sample, respectively. The curve for the mixture is the averaged response to H-fields applied along all three  $\langle 110 \rangle$  directions, which essentially reproduces the average curve in Fig. 3b. Comparing to the responses of single-phase crystals simulated under the same conditions, the strain response of a two-phase mixture is significantly enhanced, especially at small H-field.